Nanoscale

PAPER

View Article Online
View Journal | View Issue

Cite this: *Nanoscale*, 2017, **9**, 11214

Transferrin-coated magnetic upconversion nanoparticles for efficient photodynamic therapy with near-infrared irradiation and luminescence bioimaging†

Dan Wang,[a,c] Lin Zhu,[b] Yuan Pu,*[a,d] Jie-Xin Wang,[a,d] Jian-Feng Chen[a,d] and Liming Dai*[c]

Received 27th April 2017,
Accepted 25th June 2017

DOI: 10.1039/c7nr03019c

rsc.li/nanoscale

In the present study, we devised a green-synthesis route to $NaYF_4$:Gd^{3+},Yb^{3+},Er^{3+} upconversion nanoparticles (UCNPs) by using eco-friendly paraffin liquid, instead of 1-octadecene, as a high boiling non-coordinating solvent. A multifunctional nanoplatform was then developed by coating UCNPs with biocompatible transferrin (TRF) for magnetically-assisted and near-infrared light induced photodynamic therapy and bioimaging. Protoporphyrin IX (PpIX), a clinically approved photodynamic therapy agent, was loaded into the shell layer of the TRF-coated UCNPs (UCNP@TRF nanoparticles), which can be efficiently taken up by cancer cells for photodynamic therapy. Upon near-infrared light irradiation, the UCNP@TRF-PpIX nanoparticles could not only kill the cancer cells *via* photodynamic therapy but also serve as imaging probes. We also demonstrated that an external magnetic field could be used to increase the uptake of UCNP@TRF-PpIX nanoparticles by MDA-MB-231 and HeLa cancer cells, and hence result in an enhanced photodynamic therapy efficiency. This work demonstrates the innovative design and development of high-performance multifunctional PDT agents.

Introduction

Theranostics based on multifunctional nanoplatforms have recently attracted increasing attention.[1] In particular, a large variety of nanoparticle-based theranostic agents, including semiconductor quantum dots (QDs),[2] silica nanoparticles,[3] organic nanomicelles/nanodots,[4,5] metal nanoparticles,[6,7] carbon nanomaterials,[8–10] and rare-earth doped upconversion nanoparticles (UCNPs),[11,12] have been developed for bioimaging and therapy applications. Among them, UCNPs, which convert low energy near-infrared (NIR) light to high-energy ultraviolet or visible light, are of particular interest in biomedical research.[13–15] In comparison with traditional fluorescent probes, such as organic dyes[4,5] and quantum dots (QDs),[16] the UCNPs utilize NIR excitation that can significantly enhance penetration depths and minimize background autofluorescence of biological tissues, serving as ideal probes for optical imaging.[17] In addition to bioimaging, UCNPs have also been used for drug delivery and therapy in living cells and animals.[18,19] Indeed, photosensitizers, chemotherapy drugs, metal nanoparticles or graphene oxides have been loaded on the surface of UCNPs for dual imaging and therapy applications.[20–23]

$NaYF_4$:Yb^{3+},Er^{3+} is one of the most efficient NIR-to-visible up-conversion phosphors.[24] The fabrication of small $NaYF_4$:Yb^{3+},Er^{3+} nanoparticles and their surface functionalization are critical as the nanoparticles can be taken up by cells or malignant tissues (*e.g.*, tumors) for bioimaging and/or drug delivery. To date, a variety of surface functionalization methods, including silica coating,[25] polyethylene glycol (PEG) modification[26] and biomolecule conjugation,[27] just to name a few,[28] have been developed for the preparation of surface-functionalized biocompatible UCNPs. Owing to its good biocompatibility and tumor targeting ability,[29–31] transferrin (TRF, a serum protein) is attractive for the surface functionalization of nanoparticles.[32] The expected advantages of transferrin–drug conjugates include, but not limited to, a preferable tissue dis-

[a]*Beijing Advanced Innovation Center for Soft Matter Science and Engineering, State Key Laboratory of Organic-Inorganic Composites, Beijing University of Chemical Technology, Beijing 100029, China. E-mail: puyuan@mail.buct.edu.cn*
[b]*Institute of Advanced Materials for Nano-bio Applications, School of Ophthalmology and Optometry, Wenzhou Medical University, 270 Xueyuan Xi Road, Wenzhou, Zhejiang, China*
[c]*Center of Advanced Science and Engineering for Carbon (Case4Carbon), Department of Macromolecular Science and Engineering, Case Western Reserve University, Cleveland, OH 44106, USA. E-mail: liming.dai@case.edu*
[d]*Research Center of the Ministry of Education for High Gravity Engineering and Technology, Beijing University of Chemical Technology, Beijing 100029, China*
†Electronic supplementary information (ESI) available. See DOI: 10.1039/c7nr03019c

tribution, prolonged half-life of the drug in the plasma, and controlled drug release from the conjugates.[33] To the best of our knowledge, however, transferrin-coated UCNPs have not been reported.

In the present paper, we reported the synthesis of TRF-coated $NaYF_4$:Gd^{3+},Yb^{3+},Er^{3+} nanoparticles *via* a green route by using oleic acid as the surfactant and paraffin liquid as the solvent. The TRF-coating imparted high aqueous dispersibility and tumor targeting ability to the resultant nanoparticles,[34,35] which was also used as a platform to load drugs for multifunctional applications. In this context, we loaded protoporphyrin IX (PpIX), a clinically approved photodynamic therapy (PDT) agent,[36] into the TRF layer of the UCNP@TRF nanoparticles. UCNP@TRF-PpIX nanoparticles thus produced could serve as not only an upconversion luminescence imaging probe but also as an effective NIR-induced PDT agent. We also demonstrated that the PDT efficiency could be further enhanced by magnetically-assisted capture of UCNP@TRF nanoparticles into cells. This work opens new avenues for the development of high-performance multifunctional PDT agents.

Experimental

Materials and instruments

Lanthanide oxides (Er_2O_3, Yb_2O_3, Gd_2O_3 and Y_2O_3), hydrochloric acid, paraffin liquid, oleic acid, NaOH, NH_4F, tetrahydrofuran, transferrin (TRF), glutaraldehyde, and protoporphyrin IX (PpIX) were purchased from Sigma-Aldrich. All lanthanide oxides were of 99.9% or higher purity and used as received without further purification unless otherwise mentioned. Cell-culture products were purchased from Invitrogen. Deionized (DI) water was used throughout the experiment.

Transmission electron microscopy (TEM) images were recorded on a TEM unit (JEOL JEM-1230) operating at 160 kV in a bright-field mode. Powder X-ray diffraction (XRD) patterns were recorded on a MiniFlex II benchtop X-ray diffractometer at room temperature (21 °C). A 980 nm continuous wave laser (LWIR980 nm, Beijing Laserwave Optoelectronics Technology Co., Ltd) was utilized for the excitation of the UCNPs and the luminescence spectra were recorded with an optical fiber spectrometer (PG2000-Pro-EX, Ideaoptics Instruments Ltd). Fourier transform infrared (FTIR) spectra were collected using a PerkinElmer spectrum GX FTIR system. A TA Instrument with a heating rate of 10 °C was used for the thermogravimetric analysis (TGA). The absorbance spectra were recorded by using a Shimadzu UV 1800 scanning spectrophotometer. Dynamic light scattering (DLS) analysis was conducted at room temperature using a Zetasizer Nano ZS90 from Malvern Instruments Ltd.

Synthesis of $NaYF_4$:Gd^{3+},Yb^{3+},Er^{3+} nanoparticles

The $NaYF_4$:Gd^{3+},Yb^{3+},Er^{3+} nanoparticles were synthesized according to a previously reported method[37] with some modifications. In a typical experiment, Y_2O_3 (0.1 mmol), Yb_2O_3 (0.036 mmol), Gd_2O_3 (0.06 mmol), Er_2O_3 (0.004 mmol), and hydrochloric acid (30 mL, 10 wt%) were added to a 100 mL round bottom flask. The mixture was heated to 80 °C under vigorous stirring. After the solution became clear and colorless, it was then heated to 100 °C under reduced pressure to remove water and excess hydrochloric acid. The resulting solid mass was re-dispersed in 2 mL of methanol in a 50 mL flask. Thereafter, 3 mL oleic acid and 7 mL paraffin liquid were added and the solution mixture was heated to 160 °C for 30 min under vigorous stirring, followed by cooling down to room temperature. Then, 5 mL methanol solution containing 1.6 mmol NH_4F and 1 mmol NaOH was added and the solution was stirred for 30 min. After maintaining the solution at 120 °C for 30 min to evaporate the methanol, the solution was then heated to 250 °C under argon for 1.5 h to produce $NaYF_4$:Gd^{3+},Yb^{3+},Er^{3+} nanoparticles. The resulting solution was cooled down to room temperature and the UCNPs were precipitated upon the addition of ethanol, collected by centrifugation, washed with methanol and ethanol three times, and finally dried in a vacuum.

Preparation of transferrin coated $NaYF_4$:Gd^{3+},Yb^{3+},Er^{3+} nanoparticles

In a typical experiment, 5 mL tetrahydrofuran solution containing 1 mg UCNPs were added dropwise to a 5 mL aqueous solution of TRF (2 mg mL^{-1}) under sonication at room temperature, leading to the adsorption of TRF onto the UCNPs. The obtained TRF-adsorbed UCNPs were then centrifuged and washed with water 3 times to remove the unadsorbed TRF. After that, the precipitates were re-dispersed in 5 mL of water and 5 μL of glutaraldehyde solution (25%) was added to cross-link the TRF on the surface of UCNPs at room temperature for 4 h, followed by three times centrifugation and washing in water. The final product of TRF coated UCNPs (UCNP@TRF nanoparticles) was dried in a 40 °C vacuum.

Cytotoxicity and histological analyses

The mouse fibroblast cell lines (NIH-3T3) and human glioma cell lines (SHG44) were used for cytotoxicity studies of UCNP@TRF nanoparticles. Typically, the cells were seeded in 12-well plates, and treated with UCNP@TRF nanoparticles at a 1 : 40 ratio (50 μL UCNP@TRF nanoparticles in 2 mL DMEM medium). At different stages during the post treatment (0, 24, and 48 h), the cells were detached with 0.25% trypsin-EDTA and the average numbers of cells were measured by using a Z1 Coulter Particle Counter (Beckman Coulter). The cells without UCNP@TRF nanoparticle treatment were also investigated as a control group.

Potential long-time *in vivo* toxicity of UCNP@TRF nanoparticles in mouse was evaluated through histological analysis and physical/neurological evaluations. Typically, 10 mice (BALB/c) were randomly divided into two groups. For one group, UCNP@TRF nanoparticles (200 μL per mouse, 1 mg mL^{-1} in PBS) nanoparticles were intravenously injected into the mice. For the other group, the mice were injected with 200 μL PBS as a control. Physical and neurological evaluations

were performed on the mice for 60 days, and no change in weight, shape, eating, drinking, exploratory behavior or activity was observed. After 60 days, the mice were sacrificed, and their major organs (heart, liver, spleen, lung, and kidney) were removed for histological analyses. The tissues were fixed in 10% formalin, embedded in paraffin, sectioned and stained with hematoxylin and eosin. The histological sections were imaged under an inverted optical microscope.

Loading of PpIX at transferrin coated $NaYF_4$:Gd^{3+},Yb^{3+},Er^{3+} nanoparticles

1 mg of UCNP@TRF nanocomposites was dispersed in 5 mL water, followed by the addition of 10 μmol PpIX. The solution mixture was placed at 4 °C in the dark for 12 h under stirring. Excess PpIX molecules were removed by centrifugation and ethanol washing. The obtained PpIX loaded UCNP@TRF nanocomposites (*i.e.* UCNP@TRF-PpIX) were stored at 4 °C in the dark. UV-Vis absorbance spectra of the products were measured to determine the loading concentrations of PpIX. The amount of excess PpIX was determined by their characteristic absorbance peak at 545 nm. And the amount of PpIX loaded onto UCNP@TRF nanoparticles was calculated as the difference between the original amount of PpIX and the excess amount of PpIX. The loading density of PpIX in the nanoparticles was obtained in terms of mass fraction (PpIX/[PpIX + UCNP@TRF).

Release kinetics of PpIX from UCNP@TRF-PpIX nanoparticles

Briefly, 1 mg of UCNP@TRF-PpIX nanoparticles was incubated with 1 mL Tween-20 solution (1% in DI water) at 37 °C. After certain time intervals (0, 2, 4, 6, 8, 10 and 12 h), the sample was centrifuged and the UV-vis absorbance spectrum of the supernatant was measured. The release percentage of PpIX from the UCNP@TRF-PpIX system was determined by the ratio of PpIX in the supernatant and the overall amount of PpIX loaded into 1 mg of UCNP@TRF-PpIX nanoparticles.

In vitro cell imaging and therapy

MDA-MB-231 cells (human breast cancer cell line) were cultivated in Dulbecco's minimum essential media (DMEM) with 10% fetal bovine serum (FBS), 2 mM L-glutamine, and 1% antibiotic–antimycotic solution in a carbon dioxide (5%) incubator at 37 °C. One day before the cell imaging experiments, MDA-MB-231 cells were seeded in 35 mm cultivation dishes. For upconversion luminescence imaging, the cells were treated separately with nothing, a 200 μL solution of UCNP@TRF nanoparticles (20 μg mL^{-1} in water), and a 200 μL solution of UCNP@TRF-PpIX nanoparticles, respectively. The cells were incubated with nanoparticles for 2 h at 37 °C with 5% CO_2 and then washed three times with PBS (phosphate buffered saline, 1×) and directly imaged using a laser confocal scanning microscope (Olympus, FV1000) under CW excitation at 980 nm. Two groups of MDA-MB-231 cells treated with UCNP@TRF-PpIX and UCNP@TRF nanoparticles were irradiated by a 980 nm laser for 2 min and their morphologies were recorded using an optical microscope (Nikon, E200) to determine the PDT therapy.

Magnetically-assisted photodynamic therapy

MDA-MB-231 cells were cultivated in 96-well dishes. After 1 day, UCNP@TRF-PpIX nanoparticles were added into the above wells at a final concentration of 0, 30 and 60 μg mL^{-1}, respectively. The experiments were performed in the absence and presence of a magnetic field (neodymium magnet, N38, 80 mm × 40 mm) applied beneath the culture plate. After incubation for 3 h, the culture medium in all wells was changed with fresh medium, and the cells were then irradiated by the 980 nm laser at a power density of 2 W cm^{-2} for 10 min. The cells were then incubated at 37 °C for an additional 24 h prior to MTT assay to determine the cell viabilities relative to the control untreated cells.

Results and discussion

Ultra-small UCNPs were synthesized by following a published protocol[35] for the production of oleic acid coated $NaYF_4$:Gd^{3+}, Yb^{3+},Er^{3+} nanoparticles. In our work, we have replaced the commonly used 1-octadecene, as used in the previous report, with paraffin liquid as a high boiling non-coordinating solvent for the synthesis of UCNPs. Since paraffin liquid is a more environmentally friendly and much cheaper chemical than 1-octadecene,[38,39] our modified method is of great value for both laboratory research and industrial applications. Fig. 1a shows procedures for the preparation of UCNP@TRF nanoparticles. After the UCNPs were added into the aqueous solution of TRF, the UCNPs were entangled by TRF, due to the hydrophobic interactions between UCNPs and hydrophobic domains of TRF molecules. The de-solvation process of TRF from its aqueous solution was simultaneously achieved, since the solubility of TRF was significantly reduced after the addition of tetrahydrofuran into the aqueous solution. The dispersion of UCNP@TRF nanoparticles was then obtained upon sonication. Subsequently, the TRF matrix on the surface of UCNPs was knitted together by glutaraldehyde to form a stable coating. TEM images revealed that the as-synthesized UCNP and UCNP@TRF nanoparticles were smaller than 50 nm in dimension (Fig. 1b and c). However, it is difficult to observe the thin layer of TRF on the surface of UCNPs in the TEM images due to the low electron contrast between the TRF layer and UCNPs. Nevertheless, the presence of a TRF layer on the UCNPs was confirmed by FTIR and TGA. As shown in Fig. 1d, the band peaked at 2900 cm^{-1}, arising from the stretching methylene (CH_2) in the long alkyl chain of oleic acid on the surface of UCNPs,[40] and its peak intensity decreased significantly after coating the UCNPs with TRF. Meanwhile, strong band peaks at 3286, 1650, and 1530 cm^{-1}, associated with the characteristic peaks of TRF, were observed for UCNP@TRF nanoparticles. Furthermore, TGA results in Fig. 1e indicate a significant weight loss for the UCNPs over 300–400 °C due to the elimination of oleic acid ligands. However, the weight loss

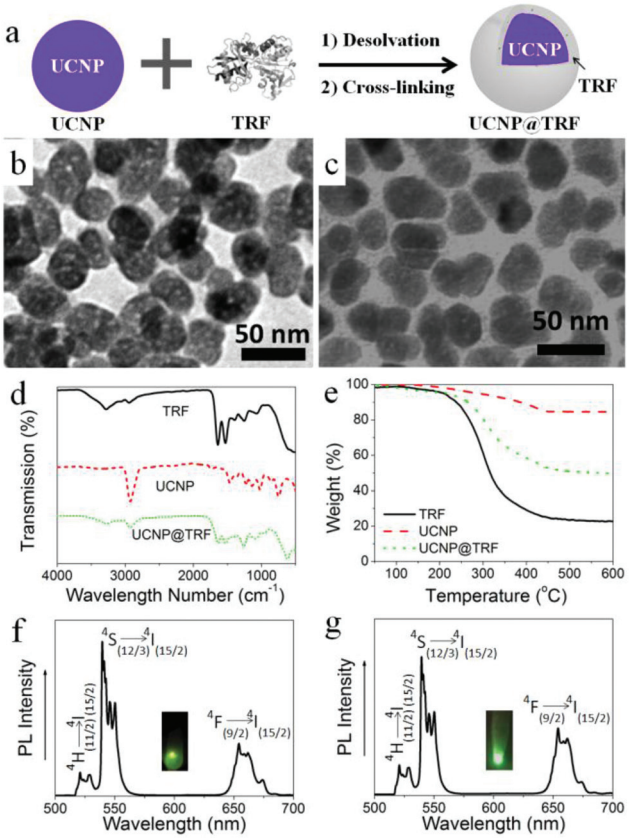

Fig. 1 (a) A schematic illustration of the fabrication of UCNP@TRF nanoparticles; TEM images of (b) UCNP and (c) UCNP@TRF nanoparticles; (d) FTIR spectra and (e) TGA curves of TRF, UCNP and UCNP@TRF nanoparticles, respectively; room temperature upconversion luminescence spectrum of 5 mg UCNPs (f) and UCNP@TRF (g) powder under NIR light excitation with a 980 nm laser at a powder density of 5 W cm^{-2}. Inset: Photographs of the UCNP and UCNP@TRF samples under NIR light excitation, respectively.

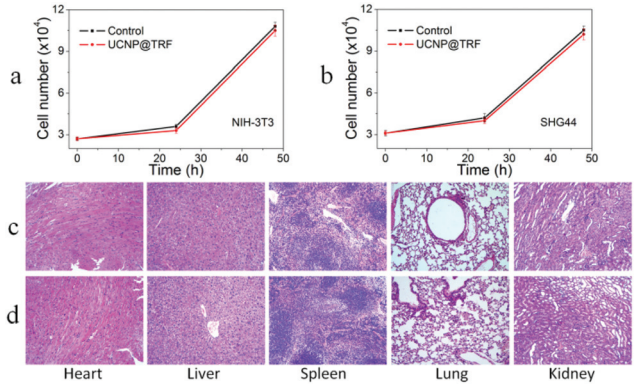

Fig. 2 Average numbers of NIH-3T3 cells (a) and SHG44 cells (b) with (red) and without (black) the addition of UCNP@TRF nanoparticles, 0 h, 24 h and 48 h post treatment; tissue sections from a mouse receiving no injection (c) and a mouse injected with UCNP@TRF nanoparticles (d) 60 days after the treatment. Major organs tested were the heart, liver, spleen, lung, and kidney.

of UCNP@TRF nanoparticles mainly occurred in the temperature range of 200–300 °C, which was associated with the loss of transferrin coated on the surface. These results demonstrate the formation of UCNP@TRF nanoparticles. Fig. 1f and g show the upconversion luminescence spectra of UCNP and UCNP@TRF nanoparticles excited by a NIR laser with a peak wavelength at 980 nm and a powder density of 5 W cm^{-2}. Both samples of UCNP and UCNP@TRF nanoparticles exhibited bright green emission, with similar luminescence spectra. The upconversion luminescence peaks at 522, 543 and 654 nm were consistent with $^2H_{11/2} \rightarrow {}^4F_{15/2}$, $^4S_{3/2} \rightarrow {}^4F_{15/2}$, and $^4F_{9/2} \rightarrow {}^4I_{15/2}$ transitions of Er^{3+}, respectively.[41]

The nature of the green synthesis, ultrafine size distribution, and NIR excited upconversion luminescence makes UCNPs of great potential for bioimaging and photodynamic therapy. Before any clinical applications could be realized, however, cytotoxicity of the resultant nanoparticles has to be studied to ensure no toxicity to normal cells or organs. Fig. 2a shows that the addition of UCNP@TRF nanoparticles didn't generate any distinct proliferation difference in either NIH-3T3 cells or SHG 44 cells even after 24 and 48 h post sample treatments. Histological analysis and physical/neurological evaluations of mice injected with UCNP@TRF nanoparticles (200 μL per mouse, 1 mg mL^{-1} in PBS) were also performed to study the potential long-time toxicity of these nanoparticles. After 60 days, the mice with (as the experimental group) and without (as the control group) intravenous injection of UCNP@TRF nanoparticles were sacrificed for histological analysis. There was no apparent tissue/cellular difference in the main organs (heart, liver, spleen, kidney or lung) between the experimental mice and the control mice (Fig. 2c). Furthermore, physical and neurological evaluations were also performed on the intravenously injected mice for more than 60 days, and no change in weight, shape, eating, drinking, exploratory behavior or activity was observed (Fig. 2d). These results indicated the potential of UCNP@TRF nanoparticles as a biocompatible nanoplatform for bio-related applications.

In some previous reports, protein modified nanoparticles have been used as loading and delivery platforms for hydrophobic molecules. For instance, Chen *et al.* have developed a multifunctional nano-platform by coating UCNPs with bovine serum albumin (BSA) derived from cows and doped two types of dye molecules into the BSA layer of the UCNP@BSA nanoparticles for imaging and therapy.[42] From the biological perspective, however, BSA is a foreign protein to human cell lines. Therefore, TRF coated nanoparticles developed in this study are more suitable as nano-platforms for bioimaging and drug delivery. Herein, we investigated the potential of using UCNP@TRF nanoparticles as a loading and delivery platform for hydrophobic molecules. Fig. 3a schematically shows the loading of PpIX molecules into the TRF layer of UCNP@TRF nanoparticles through diffusion. The amount of PpIX loaded in the UCNP@TRF-PpIX nanoparticles was calculated as the difference between the residual PpIX and original PpIX in solution determined by UV-Vis absorption measurements. The loading capacity of PpIX on UCNP@TRF nanoparticles was

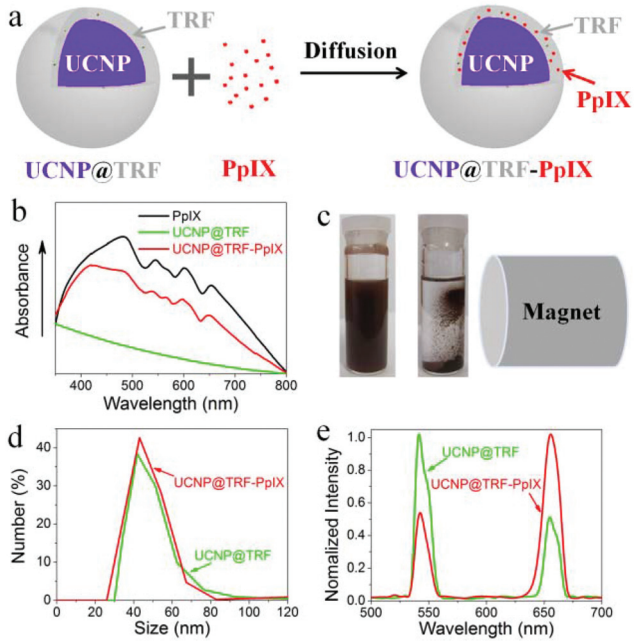

Fig. 3 (a) A schematic illustration of the fabrication of UCNP@TRF-PpIX nanocomposites; (b) absorbance spectra of PpIX (1 μg mL^{-1} in ethanol), UCNP@TRF nanoparticles (10 μg mL^{-1} in water) and UCNP@TRF-PpIX nanoparticles (10 μg mL^{-1} in water); (c) photographs of an aqueous dispersion of UCNP@TRF-PpIX nanoparticles (200 μg mL^{-1}) before and after placed one magnet (neodymium iron boron magnet, φ 1 × 2 cm) outside of the container for 3 hours; (d) DLS results of UCNP@TRF nanoparticles (50 μg mL^{-1} in water) and UCNP@TRF-PpIX nanoparticles (50 μg mL^{-1} in water); (e) normalized upconversion luminescence spectra of aqueous dispersions of UCNP@TRF nanoparticles (100 μg mL^{-1}) and UCNP@TRF-PpIX nanoparticles (100 μg mL^{-1}) excited with a 980 nm laser at powder density of 5 W cm^{-2}. The spectra were normalized by the respective maximum luminescence intensity.

evaluated to be 12.4% (PpIX/[PpIX + UCNP@TRF in wt%) at the feeding PpIX concentration of 2 mM and UCNP@TRF concentration of 0.2 mg mL^{-1}. Fig. 3b shows the absorbance spectra of PpIX, UCNP@TRF nanoparticles and UCNP@TRF-PpIX nanoparticles, respectively. As can be seen, the PpIX loaded into the TRF layer of UCNP@TRF nanoparticles remained with its characteristic absorption peaks at 485 nm, 545 nm, 602 nm and 653 nm.

As expected, an aqueous dispersion of UCNP@TRF-PpIX nanoparticles shows brown color (Fig. 3c). Due to the presence of paramagnetic Gd dopant in the nanoparticles, the UCNPs are guidable by an external magnetic field. As illustrated in Fig. 3c, the placement of a magnet bar outside of a bottle containing the aqueous dispersion of UCNP@TRF-PpIX nanoparticles for 3 h could effectively precipitate out the colored particles from the solution, indicating that PpIX molecules were indeed complexed with the UCNP@TRF nanoparticles. The DLS results showed that the loading of PpIX into UCNP@TRF nanoparticles did not cause any significant change in the particle size (Fig. 3d), suggesting that PpIX molecules indeed diffused into the TRF shell given that the UCNP is a hard core. The upconversion luminescence spectra of UCNP@TRF and UCNP@TRF-PpIX nanoparticles in aqueous solutions exhibited two peaks at 550 nm (green emission peak) and 650 nm (red emission peak) from PpIX (Fig. 3e). The intensity ratio of the green emission peak (I_G) to the red emission peak (I_R) was about 2 : 1 for UCNP@TRF nanoparticles. However, the $I_G : I_R$ was only 1 : 2 for UCNP@TRF-PpIX nanoparticles, indicating an effective energy transfer between the UCNP and PpIX molecules. The stability of PpIX in UCNP@TRF-PpIX nanoparticles was tested by release kinetics studies in Tween-20 solutions at 37 °C. As shown in Fig. S1,† the release percentage of PpIX from UCNP@TRF-PpIX nanoparticles was less than 5% during the entire time of the experiment (even after 12 h), indicating a good stability for the UCNP@TRF-PpIX system.

The photosensitization process of PpIX molecules in UCNP@TRF-PpIX nanoparticles under NIR light irradiation is shown in Fig. 4a, which shows that the UCNP converted the NIR light to high energy emission absorbed by the PpIX molecules to generate reactive oxygen species (ROS) from oxygen in air. We used 1,3-diphenylisobenzofuran (DPBF) as a chemical probe to detect the ROS generation by monitoring its diminished optical absorbance in the presence of singlet oxygen. By mixing 10 μL of DPBF (1 mM in water) with 2 mL of UCNP@TRF-PpIX nanoparticles (100 μg mL^{-1} in water), followed by irradiation with a NIR laser (980 nm, 1 W cm^{-2}) to generate ROS, we observed a continuous decrease in the optical absorption with increasing irradiation time, as exemplified by UCNP@TRF-PpIX nanoparticles (Fig. 4b). In contrast, the absorbance of DPBF showed no significant change in either PpIX dispersion or UCNP@TRF nanoparticle dispersion in the absence of PpIX under NIR irradiation (Fig. 4c). These results indicated that ROS in the UCNP@TRF-PpIX system was

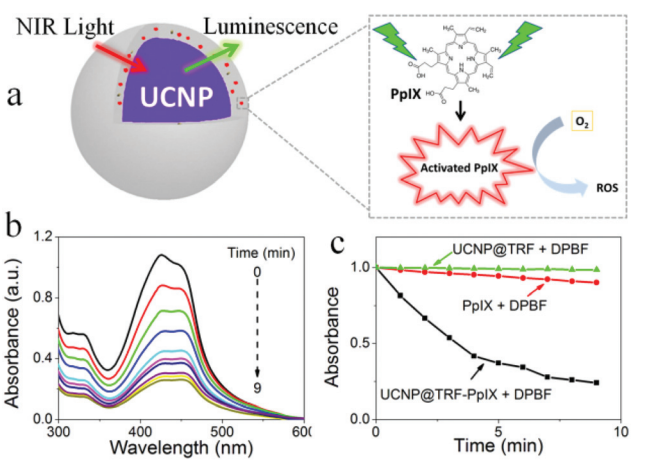

Fig. 4 (a) A schematic illustration of photosensitization of PpIX molecules under NIR light irradiation in the UCNP@TRF-PpIX system; (b) absorption spectra of DPBF under NIR light irradiation in aqueous dispersion of UCNP@TRF-PpIX nanoparticles (100 μg mL^{-1}); (c) normalized decay curves of the absorption density at 420 nm for DPBF under NIR light irradiation in 2 mL aqueous dispersions of UCNP@TRF-PpIX nanoparticles (100 μg mL^{-1}), PpIX (0.2 μg mL^{-1}), and UCNP@TRF nanoparticles (100 μg mL^{-1}), respectively.

indeed generated by irradiation of PpIX with the UCNP upper converted NIR light, as shown in Fig. 4a. The effective generation of ROS by UCNP@TRF-PpIX nanoparticles under NIR light irradiation would enable NIR-induced PDT by using these newly-developed UCNP@TRF-PpIX nanoparticles, as we shall see below.

To investigate the PDT process, we assessed the cellular uptake of UCNP@TRF-PpIX nanoparticles by *in vitro* cell imaging. MDA-MB-231 cells were seeded in 35 mm cultivation dishes contain 2 mL DMEM culture media. The cells were randomly divided into three groups. After incubation at 37 °C under 5% CO_2 for 24 h, two groups of MDA-MB-231 cells were separately treated with 200 μL aqueous dispersion of UCNP@TRF nanoparticles (20 μg mL^{-1}) and UCNP@TRF-PpIX nanoparticles (20 μg mL^{-1}) and the cells were incubated for another 2 h. The third group of cells was blank control cells without any treatment. Thereafter, all the cell samples were gently washed three times with PBS (pH = 7.4 and 10 mM) and directly imaged using a laser confocal scanning microscope (Olympus, FV1000) under excitation at 980 nm (Fig. S2†). As shown in Fig. 5, the blank cells (Fig. 5a) exhibited no upconversion luminescence signals while the cells treated with UCNP@TRF (Fig. 5b) and UCNP@TRF-PpIX nanoparticles (Fig. 5c) were remarkably stained with strong bright green emission from UCNP, indicating that both UCNP@TRF nanoparticles and UCNP@TRF-PpIX nanoparticles have penetrated through the cell membrane into the cytoplasm and perinuclear regions (Fig. S3†).

Based on the above results, we further studied NIR-induced PDT for the MDA-MB-231 cells using UCNP@TRF-PpIX nanoparticles. Two groups of the cells were treated with

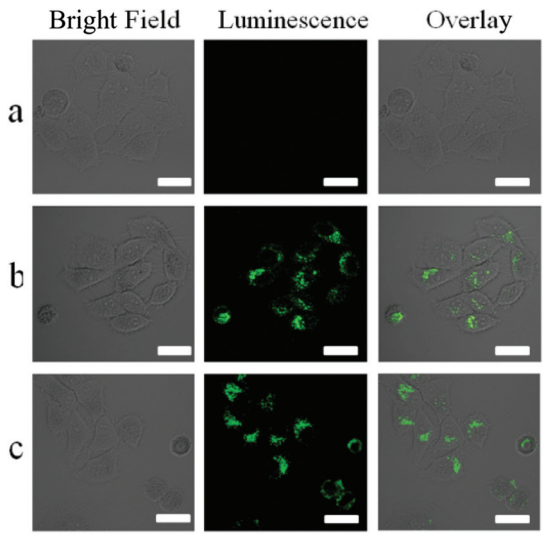

Fig. 5 *In vitro* upconversion luminescence imaging of MDA-MB-231 cells incubated in 2 mL of DMEM culture media with the addition of (a) nothing, (b) 200 μL aqueous dispersion of UCNP@TRF nanoparticles (20 μg mL^{-1}) and (c) 200 μL aqueous dispersion of UCNP@TRF-PpIX nanoparticles (20 μg mL^{-1}) for 2 h at 37 °C. The scale bar represents 50 μm.

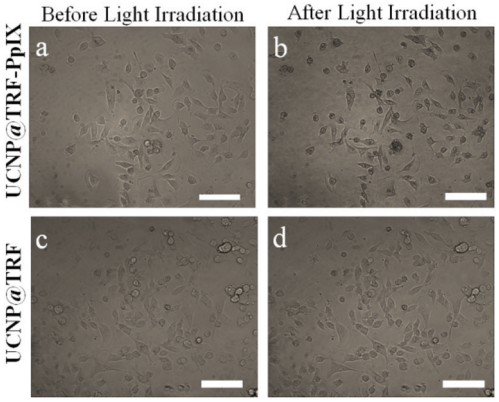

Fig. 6 Bright-field images of MDA-MB-231 cells in 2 mL DMEM culture media with the addition of UCNP@TRF-PpIX nanoparticles (a, b) and UCNP@TRF nanoparticles (c, d) before (a, c) and after (b, d) 2 min irradiation under 980 nm light, respectively. The power density of the NIR laser was 2 W cm^{-2}. The concentrations of both kinds of nanoparticles were 60 μg mL^{-1}. The scale bar represents 100 μm.

UCNP@TRF-PpIX nanoparticles and UCNP@TRF nanoparticles, respectively, and an optical microscope was used to record the morphology changes of the cells before and after the NIR irradiation (980 nm, 2 W cm^{-2}) for 2 min. The ambient temperature of the cells was measured using a digital infrared thermometer. Due to the low intensity and duration of NIR irradiation, no significant temperature change was observed. As shown in Fig. 6a and b, the MDA-MB-231 cells treated with UCNP@TRF-PpIX nanoparticles by NIR irradiation showed significant morphological changes due to the cell structure damage. However, the morphology of the cells treated with UCNP@TRF nanoparticles under the same conditions did not change (Fig. 6c and d). These results demonstrated that the ROS generation from UCNP@TRF-PpIX nanoparticles under NIR irradiation was responsible for the observed cancer cell destruction.

The magnetic properties of UCNP@TRF-PpIX nanoparticles are an additional advantage for their PDT application as the use of an external magnetic field could enhance the cellular uptake of the nanoparticles. Fig. 6a schematically shows the magnetic enhanced cellular uptake of UCNP@TRF-PpIX nanoparticles. In the absence of a magnetic field, the UCNP@TRF-PpIX nanoparticles were well suspended in the cell culture medium and the cellular uptake of the nanoparticles depended mainly on the random dispersion of the UCNP@TRF-PpIX nanoparticles towards the cells. In the presence of a magnetic field, however, the UCNP@TRF-PpIX nanoparticles were subjected to a downward force towards the magnet underneath the culture dish, leading to an improved contact of UCNP@TRF-PpIX nanoparticles with the cells, and hence an enhanced cellular uptake (Fig. 7a and b). The ambient temperature of the cells was measured using a digital infrared thermometer to investigate the magnetic heating effect of the magnetic UCNP nanoparticles. No significant temperature change was observed due to the low magnetic

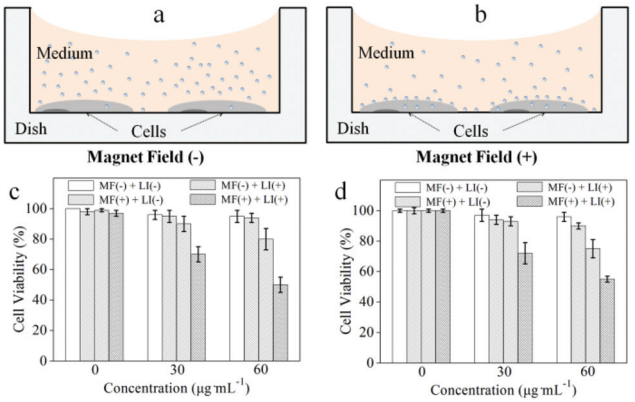

Fig. 7 Different particle endocytosis and intracellular delivery in the (a) absence (MF(–)) and (b) presence (MF(+)) of an external magnetic field, respectively; cell viability of (c) MDA-MB-231 cells and (d) HeLa cells treated with UCNP@TRF-PpIX nanoparticles at various concentrations (0, 30 and 60 μg mL^{-1}) in the absence and presence of an external magnetic field and 980 nm laser irradiation (2 W cm^{-2}). MF: magnetic field; LI: light irradiation; absence (–); presence (+).

field intensity used in the present study. The cell viability of MDA-MB-231 cells treated with UCNP@TRF-PpIX nanoparticles (60 μg mL^{-1}) under the NIR irradiation in the absence of an external magnetic field was found to be about 80%. In the presence of an external magnetic field (neodymium magnet, N38, 80 mm × 40 mm), however, the cell viabilities for MDA-MB-231 cells treated with UCNP@TRF-PpIX nanoparticles of 30 μg mL^{-1} and 60 μg mL^{-1} under the NIR irradiation were determined to be 70% and 50%, respectively. Fig. 7c shows the cell viabilities for MDA-MB-231 cells treated with UCNP@TRF-PpIX nanoparticles under various conditions. These results clearly indicate a significantly enhanced PDT efficiency under an external magnetic field. Similar studies were performed by using HeLa cells. As shown in Fig. 7d, the cell viability of HeLa cells decreased after the treatment of UCNP@TRF-PpIX nanoparticles and NIR irradiation due to the efficient PDT of UCNP@TRF-PpIX nanoparticles. The PDT efficiency of UCNP@TRF-PpIX nanoparticles for HeLa cells could also be enhanced by using an external magnetic field. These results demonstrated the nanoplatform developed in this study can be applied to different types of cancers.

Conclusions

UCNPs were synthesized *via* a green approach by using paraffin liquid as a high boiling non-coordinating solvent. Transferrin (*i.e.*, TRF) coated $NaYF_4$:Gd^{3+},Yb^{3+},Er^{3+} upconversion nanoparticles (*i.e.*, UCNP@TRF) were then developed as a nanoplatform for bio-related applications. While the UCNP core converts NIR light into visible luminescence, the TRF shell serves as a delivery platform to load molecules/drugs for therapy. In this context, we have loaded PpIX onto UCNP@TRF nanoparticles to produce UCNP@TRF-PpIX nanoparticles for NIR light induced PDT of cancer cells and biomedical imaging. Furthermore, we demonstrated the magnetic-enhanced PDT efficiency of the UCNP@TRF-PpIX nanoparticles doped with paramagnetic Gd dopants. This work represents a new strategy for the design and development of high-performance multifunctional PDT agents. The use of the more environmentally friendly and much cheaper paraffin than the commonly used 1-octadecene should facilitate the scale up of this newly-developed approach.

Acknowledgements

We are grateful for financial support from the National Key R&D Program of China (2016YFA0201701/2016YFA0201700), National Natural Science Foundation of China (51641201, 201620102007, 21622601), Fundamental Research Funds for the Central Universities (BUCTRC201601), and the "111" project of China (B14004).

Notes and references

1 T. Sun, Y. Zhang, B. Pang, D. Hyun, M. Yang and Y. Xia, *Angew. Chem., Int. Ed.*, 2014, **53**, 12320–12364.
2 B. A. Kairdolf, T. H. Stokes, M. D. Wang, A. N. Young and S. M. Nie, *Annu. Rev. Anal. Chem.*, 2013, **6**, 143–162.
3 J. Qian, D. Wang, F. Cai, Q. Zhan, Y. Wang and S. He, *Biomaterials*, 2012, **33**, 4851–4860.
4 X. Zhang, K. Wang, M. Liu, X. Zhang, L. Tao, Y. Chen and Y. Wei, *Nanoscale*, 2015, **7**, 11486–11508.
5 D. Wang, J. Qian, W. Qin, A. Qin, B. Z. Tang and S. He, *Sci. Rep.*, 2014, **4**, 4279.
6 N. C. Bigall, W. J. Parak and D. Dorfs, *Nano Today*, 2012, **7**, 282–296.
7 E. Peng, E. S. G. Choo, C. S. H. Tan, X. Tang, Y. Sheng and J. Xue, *Nanoscale*, 2013, **5**, 5994–6005.
8 D. Wang, J.-F. Chen and L. Dai, *Part. Part. Syst. Charact.*, 2015, **5**, 515–523.
9 D. Wang, L. Zhu, J.-F. Chen and L. Dai, *Nanoscale*, 2015, **7**, 9894–9901.
10 D. Wang, L. Zhu, C. McCleese, C. Bruda, J.-F. Chen and L. Dai, *RSC Adv.*, 2016, **6**, 41516–41521.
11 B. Zhou, B. Shi, D. Jin and X. Liu, *Nat. Nanotechnol.*, 2015, **10**, 924–936.
12 G. Y. Chen, H. L. Qiu, P. N. Prasad and X. Y. Chen, *Chem. Rev.*, 2014, **114**, 5161–5214.
13 D. Wang, L. Zhu, J.-F. Chen and L. Dai, *Angew. Chem., Int. Ed.*, 2016, **55**, 10795–10799.
14 B. Liu, C. Li, P. Ma, Y. Chen, Y. Zhang, Z. Hou, S. Huang and J. Lin, *Nanoscale*, 2015, **7**, 1839–1848.
15 C. Chen, N. Kang, T. Xu, D. Wang, L. Ren and X. Q. Guo, *Nanoscale*, 2015, **7**, 5249–5261.
16 D. Wang, J. Liu, J.-F. Chen and L. Dai, *Adv. Mater. Interfaces*, 2016, **3**, 1500439.
17 J. Zhou, Z. Liu and F. Li, *Chem. Soc. Rev.*, 2012, **41**, 1323–1349.
18 D. Yang, P. A. Ma, Z. Hou, Z. Cheng, C. Li and J. Lin, *Chem. Soc. Rev.*, 2014, **44**, 1416–1448.

19 L. Prodi, E. Rampazzo, F. Rastrelli, A. Speghini and N. Zaccheroni, *Chem. Soc. Rev.*, 2015, **44**, 4922–4952.
20 N. M. Idris, M. K. Gnanasammandhan, J. Zhang, P. C. Ho, R. Mahendran and Y. Zhang, *Nat. Med.*, 2012, **18**, 1580–1585.
21 L. Cheng, K. Yang, Y. G. Li, J. H. Chen, C. Wang, M. W. Shao, S. T. Lee and Z. Liu, *Angew. Chem., Int. Ed.*, 2011, **50**, 7385–7390.
22 L. P. Qian, L. H. Zhou, H.-P. Too and G.-M. Chow, *J. Nanopart. Res.*, 2011, **13**, 499–510.
23 Y. H. Wang, H. G. Wang, D. P. Liu, S. Y. Song, X. Wang and H. J. Zhang, *Biomaterials*, 2013, **34**, 7715–7724.
24 K. W. Krämer, D. Biner, G. Frei, H. U. Güdel, M. P. Hehlen and S. R. Lüthi, *Chem. Mater.*, 2004, **16**, 1244–1251.
25 H. S. Qian, H. C. Guo, P. C. L. Ho, R. Mahendran and Y. Zhang, *Small*, 2009, **5**, 2285–2290.
26 J. C. Boyer, M. P. Manseau, J. I. Murray and F. C. J. M. van Veggel, *Langmuir*, 2010, **26**, 1157–1164.
27 Q. Q. Zhan, J. Qian, H. J. Liang, G. Somesfalean, D. Wang, S. L. He, Z. G. Zhang and S. Andersson-Engels, *ACS Nano*, 2011, **5**, 3744–3757.
28 C. Wang, L. Cheng and Z. Liu, *Theranostics*, 2013, **3**, 317–330.
29 J. Y. Yhee, S. J. Lee, S. Lee, S. Song, H. S. Min, S.-W. Kang, S. Son, S. Y. Jeong, I. C. Kwon, S. H. Kim and K. Kim, *Bioconjugate Chem.*, 2013, **24**, 1850–1860.
30 D. T. Wiley, P. Webster, A. Gale and M. E. Davis, *Proc. Natl. Acad. Sci. U. S. A.*, 2013, **110**, 8662–8667.
31 S. Dixit, T. Novak, K. Miller, Y. Zhu, M. E. Kenney and A.-M. Broome, *Nanoscale*, 2015, **7**, 1782–1790.
32 A. Vincent, S. Babu, E. Heckert, J. Dowding, S. M. Hirst, T. M. Inerbaev, W. T. Self, C. M. Reilly, A. E. Masunov, T. S. Rahmanm and S. Seal, *ACS Nano*, 2009, **3**, 1203–1211.
33 H. Li, H. Sun and Z. M. Qian, *Trends Pharmacol. Sci.*, 2002, **23**, 206–209.
34 A. S. Pitek, D. O'Connell, E. Mahon, M. P. Monopoli, F. B. Bombelli and K. A. Dawson, *PLoS One*, 2012, **7**, e40685.
35 P. D. Pino, B. Pelaz, Q. Zhang, P. Maffre, G. U. Nienhaus and W. J. Parak, *Mater. Horiz.*, 2014, **1**, 301–313.
36 A. B. Ormond and H. S. Freeman, *Materials*, 2013, **6**, 817–840.
37 F. Wang, Y. Han, C. S. Lim, Y. H. Lu, J. Wang, J. Xu, H. Y. Chen, C. Zhang, M. H. Hong and X. G. Liu, *Nature*, 2010, **463**, 1061–1065.
38 D. Wang, J. Qian, F. Cai, S. He, S. Han and Y. Mu, *Nanotechnology*, 2012, **23**, 245701.
39 Z. Deng, L. Cao, F. Tang and B. Zou, *J. Phys. Chem. B*, 2005, **109**, 16671–16675.
40 Z. G. Chen, H. L. Chen, H. Hu, M. X. Yu, F. Y. Li, Q. Zhang, Z. G. Zhou, T. Yi and C. H. Huang, *J. Am. Chem. Soc.*, 2008, **130**, 3023–3029.
41 L. Xiong, Z. Chen, Q. Tian, T. Cao, C. Xu and F. Li, *Anal. Chem.*, 2009, **81**, 8687–8694.
42 Q. Chen, C. Wang, L. Cheng, W. W. He, Z. P. Cheng and Z. Liu, *Biomaterials*, 2014, **35**, 2915–2923.